ACS APPLIED MATERIALS & INTERFACES

Research Article

www.acsami.org

Substantial Oxygen Flux in Dual-Phase Membrane of Ceria and Pure Electronic Conductor by Tailoring the Surface

Jong Hoon Joo,*[,†] Kyong Sik Yun,[†] Jung-Hwa Kim,[‡] Younki Lee,[†,§] Chung-Yul Yoo,[†] and Ji Haeng Yu*[,†]

[†]Advanced Materials & Devices Laboratory, Korea Institute of Energy Research, 152 Gajeong-ro, Daejeon 305-343, Republic of Korea

[‡]Platform Technology Laboratory, Samsung Electronics, 130 Samsung-ro, Yeongtong-gu, Suwon-si, Gyeonggi-do 443-803, Republic of Korea

ABSTRACT: The oxygen permeation flux of dual-phase membranes, $Ce_{0.9}Gd_{0.1}O_{2-\delta}$–$La_{0.7}Sr_{0.3}MnO_{3\pm\delta}$ (GDC/LSM), has been systematically studied as a function of their LSM content, thickness, and coating material. The electronic percolation threshold of this GDC/LSM membrane occurs at about 20 vol % LSM. The coated LSM20 (80 vol % GDC, 20 vol % LSM) dual-phase membrane exhibits a maximum oxygen flux of 2.2 mL·cm^{-2}·min^{-1} at 850 °C, indicating that to enhance the oxygen permeation flux, the LSM content should be adjusted to the minimum value at which electronic percolation is maintained. The oxygen ion conductivity of the dual-phase membrane is reliably calculated from oxygen flux data by considering the effects of surface oxygen exchange. Thermal cycling tests confirm the mechanical stability of the membrane. Furthermore, a dual-phase membrane prepared here with a cobalt-free coating remains chemically stable in a CO_2 atmosphere at a lower temperature (800 °C) than has previously been achieved.

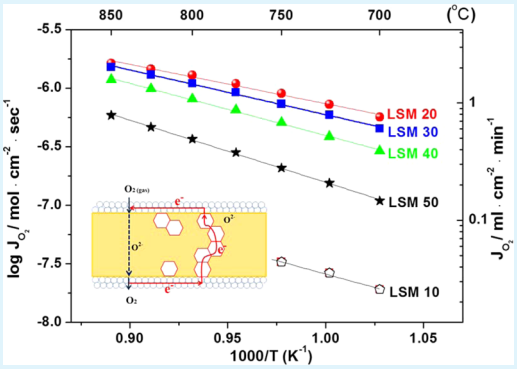

KEYWORDS: *dual-phase membrane, oxygen permeation, fluorite, perovskite, percolation*

1. INTRODUCTION

Oxyfuel technology has attracted considerable attention since it promises to capture the CO_2 emitted by coal-fired power stations. However, the overall efficiency of oxyfuel combustion is limited by the high cost of oxygen generation by cryogenic distillation.[1,2] Ceramic oxygen transport membranes have been studied as a promising alternative to cryogenic oxygen supply.[3] Single-phase perovskite materials containing Co and Fe are particularly interesting because of their high oxygen permeability and their controllable properties. These materials have high oxygen ionic conductivities at elevated temperatures due to the high oxygen vacancy concentration and mobility therein.[4,5] However, their chemical and mechanical instability when exposed to atmospheres containing, for example, CO_2 and a large oxygen partial pressure gradient is a major obstacle for their industrial application.[6−8] Simultaneously achieving high oxygen fluxes and a high stability is indeed extremely difficult with single-phase perovskites. Recently, dual-phase membranes that consist of an electrolyte oxide and a perovskite material have been developed to overcome these shortcomings while maintaining a high permeability to oxygen.[9−14] Dual-phase membranes whose electronic conductor phase has a high ionic conductivity, $(Ba,Sr)(Co,Fe)O_{3-\delta}$ for example,[15] typically exhibit high oxygen permeability. However, the applicability of this type of membrane is questionable due to the chemical and mechanical instability of the electronic conductor under operating conditions. Generally, the number of oxygen vacancies in permeable perovskite materials increases with decreasing oxygen partial pressure (Po_2) and increasing temperature. The difference in Po_2 between the feed and sweep sides of the membrane induces an oxygen deficiency gradient, which in turn leads to chemical expansion because the volume of the unit cell increases as the valence states of the transition metals therein decrease.[16] This chemically induced stress in membranes exposed to a Po_2 gradient can lead to fracture or cracking.

Among a number of possible combinations for dual-phase membranes, associating an acceptor-doped ceria with lanthanum strontium manganite (LSM) is promising, because the latter is more stable, both mechanically and chemically, than other perovskites due to the near absence of oxygen vacancies ($\delta \approx 0$) at intermediate oxygen partial pressures (10^{-5} to 10^{-10} atm) and elevated temperatures (600−1000 °C).[17] In addition, the thermal expansion coefficients (TECs) of doped ceria (12.8×10^{-6} K^{-1} at 50−1000 °C)[18] and LSM (12.3×10^{-6} K^{-1} at 800 °C)[19] are similar (less than 4% difference), which should guarantee the mechanical strength of the composite during thermal cycling. These advantages in terms of stability notwithstanding, dual-phase membranes consisting of an acceptor doped ceria and a pure electronic oxide typically have a low oxygen permeability, the negligible oxygen ion conductivity of the electronic oxide forming a barrier to oxygen

Received: March 15, 2015
Accepted: June 17, 2015
Published: June 17, 2015

DOI: 10.1021/acsami.5b03392
ACS Appl. Mater. Interfaces 2015, 7, 14699−14707

diffusion. Furthermore, the permeation flux through ceria-based dual-phase membranes such as gadolinium-doped ceria (GDC)/LSM composites has been reported to be 10 times lower than expected due to interdiffusion of the constituents.[20] However, our previous work shows that the ionic conductivity reported for composite membranes may be underestimated due to surface-exchange kinetics having been ignored. Moreover, lowering the electronic conductor content of dual-phase membranes to ca. 20 vol %, lower than typically reported in the literature should allow substantial oxygen flux.[10]

In this work, the oxygen permeation flux in GDC/LSM ($Ce_{0.9}Gd_{0.1}O_{2-\delta}$/$La_{0.7}Sr_{0.3}MnO_{3\pm\delta}$) composites has been studied systematically as a function of the concentration of the two phases, to understand the role of GDC. Furthermore, the effects on the flux and the surface-exchange kinetics of different coating materials and membrane thickness were investigated. Reliable estimates of the ionic conductivity in the GDC/LSM composite membrane are obtained by including surface-exchange effects. Thermal cycling tests and permeation experiments under a pure CO_2 atmosphere were also performed to verify the mechanical and chemical stability of these coated dual-phase membranes.

2. EXPERIMENTAL SECTION

The GDC/LSM dual-phase membranes were fabricated by tape casting and lamination. A mixture of $Ce_{0.9}Gd_{0.1}O_{2-\delta}$ (Anan Kasei, Anan, Japan) and $La_{0.7}Sr_{0.3}MnO_{3\pm\delta}$ (Kceracell, Daejeon, Korea) was homogenized by ball milling for 48 h in ethanol. The dried powder was then ball-milled for 24 h with appropriate amounts of plasticizer, binder, dispersant, and solvent to prepare slurries that were tape cast onto a polyethylene carrier film. The green tapes were laminated at 70 °C under a pressure of 10 MPa to control the thickness of the LSM/GDC dual-phase membrane and were sintered at 1300 °C for 3 h for densification. $La_{0.6}Sr_{0.4}CoO_{3-\delta}$ (LSC; Kceracell)—a highly active cathode material typically used with ceria electrolytes in solid-oxide fuel cells (SOFCs)—or $Sr_{0.97}Ti_{0.5}Fe_{0.5}O_{3-\delta}$ (STF; Kceracell) powders were mixed with an organic solution to coat the membrane surface. In order to characterize the surface-exchange kinetics, an LSC or STF coating slurry was brush-painted on one or both sides of the dual-phase membranes before firing at 1000 °C for 3 h. The oxygen permeation flux was measured using a gas chromatograph (ACME 6000, YoungLin) equipped with a molecular sieve column and a thermal conductivity detector. The sintered membranes were glass-sealed onto alumina tubes. Synthetic air (0.21 atm) was introduced into the feed side while He or CO_2 was fed to the permeate side of the membrane at 400 mL·min^{-1}. The measured oxygen permeation fluxes were corrected by subtracting the leakage flux. Based on the N_2 signal, oxygen leakage was less than 0.1%. The electrical conductivity of the sintered LSM/GDC membrane was measured, using a four-probe DC setup, with an electrochemical interface (Solartron, SI 1287, West Sussex, U.K.). The microstructure of the membranes and coating layer was observed by scanning electron microscopy (SEM, Hitachi, Tokyo, Japan). The crystal phase of the membranes was characterized by X-ray diffraction (XRD, Rigaku 2200), and the lattice parameters were calculated by using the FullProf program.

3. RESULTS AND DISCUSSION

Electrical Conductivities of LSM-GDC Composites. Since the oxygen ion conductivity of LSM is negligible (~10^{-7} S·cm^{-1} at 800 °C in air),[21] its concentration in the LSM/GDC dual-phase membrane should be minimized to enhance oxygen flux. Since the electrical conductivity of LSM is much higher than that of GDC, the composite should go through a percolation threshold at a given composition. In order to identify the minimum content of LSM required for electrical percolation, the conductivity of the GDC/LSM composite was measured as a function of its LSM content, as shown in Figure 1.

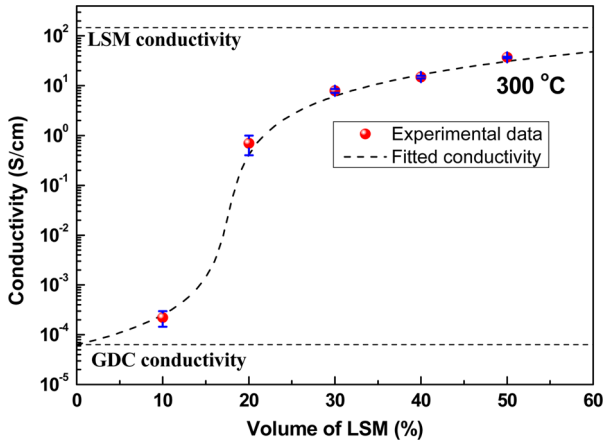

Figure 1. Electrical conductivities at 300 °C of the dual-phase GDC/LSM ($Ce_{0.9}Gd_{0.1}O_{2-\delta}$/$La_{0.7}Sr_{0.3}MnO_{3\pm\delta}$) membrane as a function of its LSM content. Error bars represent the 95% confidence interval about the mean values.

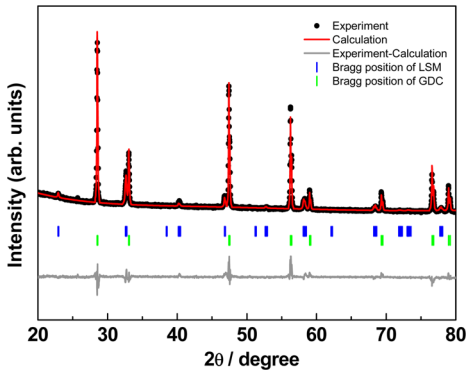

Figure 2. Room temperature X-ray diffractograms obtained for the LSM20 dual-phase membrane (80 vol % $Ce_{0.9}Gd_{0.1}O_{2-\delta}$, 20 vol % $La_{0.7}Sr_{0.3}MnO_{3\pm\delta}$).

A general effective-media equation was used to fit the conductivity behavior of the composite as follows:[22]

$$\frac{f(\sigma_l^{1/t} - \sigma_{tot}^{1/t})}{\sigma_l^{1/t} + (f_c/(1-f_c))\sigma_{tot}^{1/t}} + \frac{(1-f)(\sigma_h^{1/t} - \sigma_{tot}^{1/t})}{\sigma_h^{1/t} + (f_c/(1-f_c))\sigma_{tot}^{1/t}} = 0 \quad (1)$$

where f_c, f, and t are respectively the percolation volume fraction of the LSM phase, the LSM volume fraction, and the percolation exponent, and σ_h, σ_l, and σ_{tot} represent the conductivities of the high conductivity phase (LSM), the low conductivity phase (GDC), and the composite as a whole, respectively. The values fit in this way for the percolation exponent (t) and volume fraction (f_c) are 1.72 and 0.17, respectively, the latter indicating the effective percolation slope, which is steeper the lower t is.[23] The percolation volume fraction is found to be around 20 vol %, in good agreement with the reported value for the percolation threshold in GDC/$La_{0.6}Sr_{0.4}CoO_{3-\delta}$ (LSC) composites (~20 vol %).[24] Since the percolation behavior is also influenced to an extent by the morphology of the constituents, notably the particle size, shape, and distribution, therein 20 vol % LSM was determined to be the minimum content that guarantees electrical percolation in this composite membrane.

DOI: 10.1021/acsami.5b03392
ACS Appl. Mater. Interfaces 2015, 7, 14699−14707

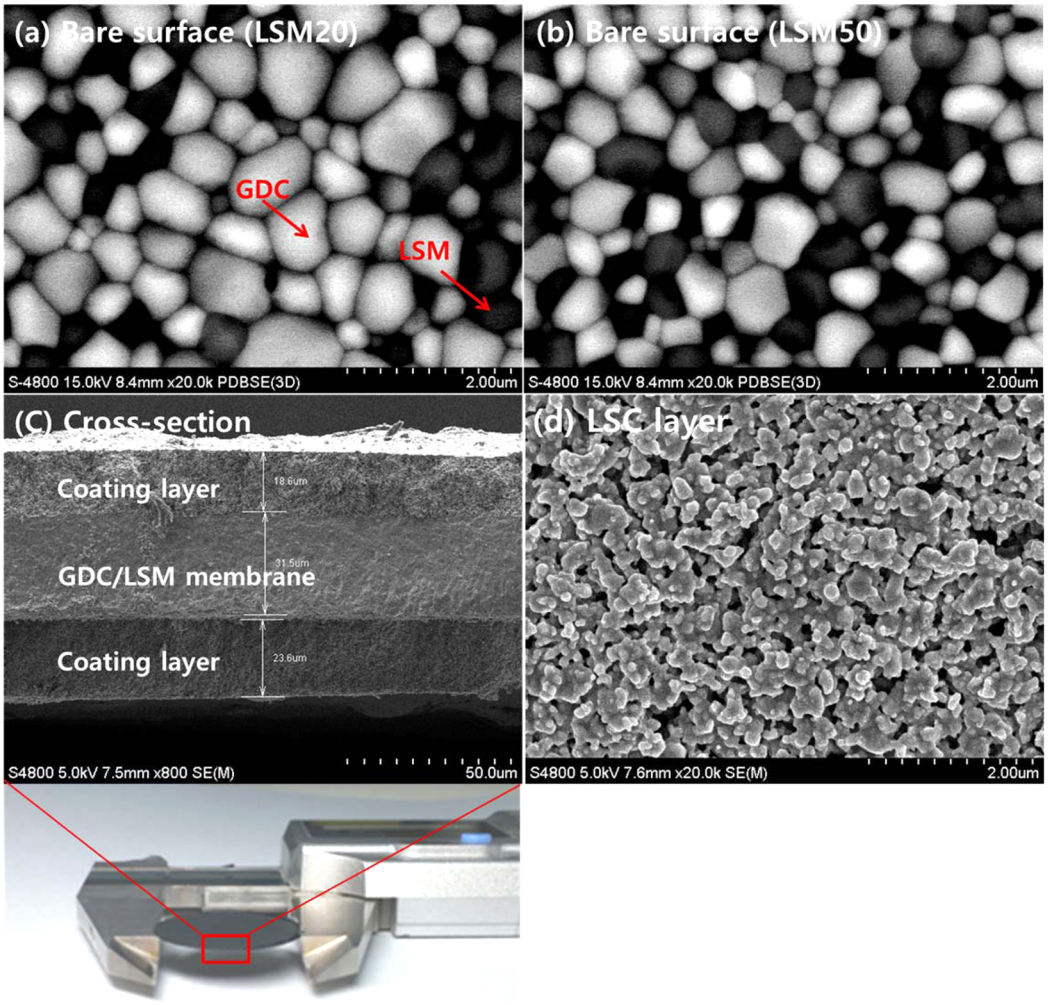

Figure 3. Scanning electron micrographs and a photoimage of dual-phase membranes: (a) bare surface of the LSM20 membrane, (b) bare surface of LSM50 membrane, (c) cross-section of the LSM20 membrane with LSC layers, and (d) surface of a porous LSC layer.

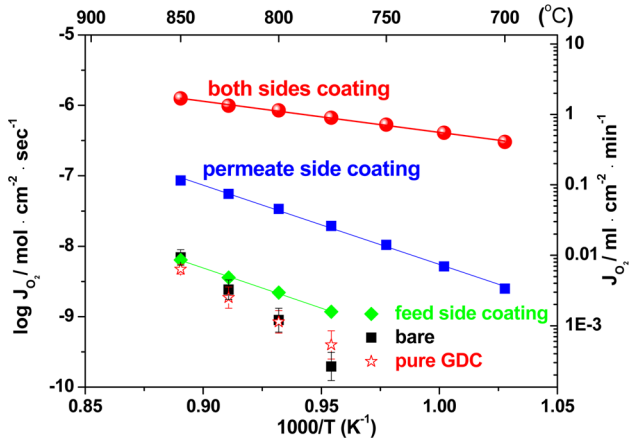

Figure 4. Oxygen permeation fluxes measured through free-standing LSM20 dual-phase membranes (~60 μm thick) with and without a porous $La_{0.6}Sr_{0.4}CoO_{3-\delta}$ coat. Fluxes of bare pure GDC (~60 μm thick) are also shown for comparison.

Figure 2 shows the Rietveld refinement of XRD patterns obtained for a sintered LSM20 (80 vol % GDC, 20 vol % LSM) dual-phase membrane. No peaks other than those for LSM and GDC are observed, indicating that any secondary phases are present in concentrations below the detection limit of routine XRD analysis. The volume of the LSM unit cell in this membrane (350.2 Å^3; *a*, 5.494 Å; *c*, 13.396 Å; space group, $R\bar{3}c$) is smaller than that in pure LSM (352.3 Å^3; *a*, 5.514 Å; *c*, 13.377 Å), while the volume of the GDC unit cell in the membrane (159.0 Å^3; *a*, 5.418 Å; space group, $Fm\bar{3}m$) is slightly larger than that in pure GDC (158.8 Å^3; *a*, 5.416 Å). The expansion of GDC unit cells has been reported elsewhere for other GDC-based composite membranes and may be caused by the diffusion of large cations (La or Sr) into the GDC during sintering.[25]

Figure 3 shows SEM images of sintered LSM20 and LSM50 (50 vol % $Ce_{0.9}Gd_{0.1}O_{2-\delta}$, 50 vol % $La_{0.7}Sr_{0.3}MnO_{3\pm\delta}$) samples, the former with and without a porous LSC coat. Since the number of backscattered electrons increases with the atomic number of the scattering atoms, the darker grains are assigned to the LSM phase. The grains in this phase range from 0.2 to 1 μm in diameter. The micrograph of the LSC-coated 30 μm thick free-standing LSM20 membrane clearly shows that the LSC layer is porous and about 20 μm thick.

Oxygen Permeation Flux of the Dual-Phase Membrane. Figure 4 shows the oxygen permeation flux measured through ~60 μm thick free-standing LSM20 dual-phase membranes with and without a porous LSC coat under an air/He gradient. Fluxes of bare pure GDC (~60 μm thick)

DOI: 10.1021/acsami.5b03392
ACS Appl. Mater. Interfaces 2015, 7, 14699−14707

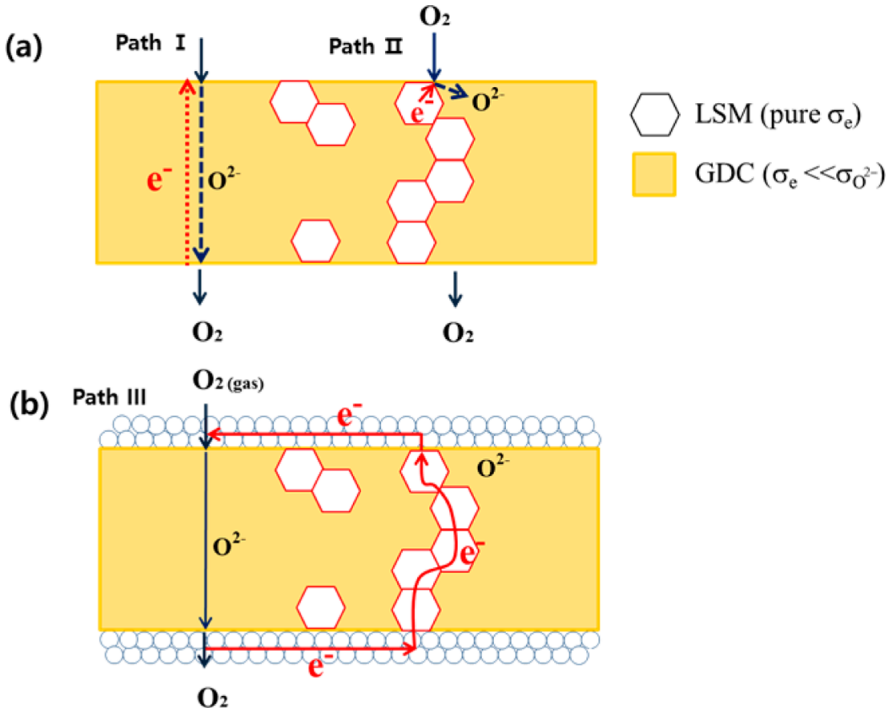

Figure 5. Possible routes for oxygen transport in (a) uncoated and (b) coated $Ce_{0.9}Gd_{0.1}O_{2-\delta}/La_{0.7}Sr_{0.3}MnO_{3\pm\delta}$ dual-phase membranes.

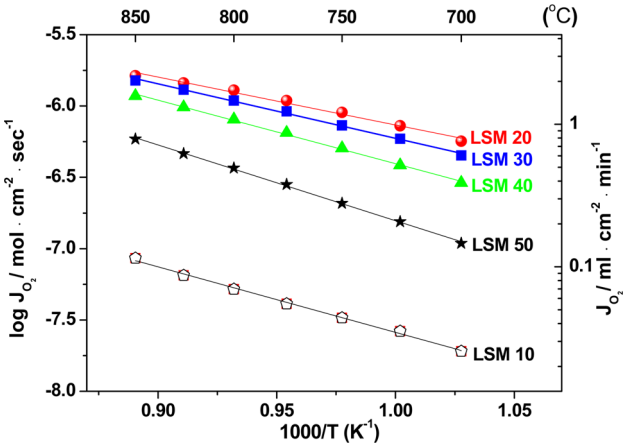

Figure 6. Temperature and LSM volume fraction dependence of the oxygen permeation flux through ~30 μm thick GDC/LSM dual-phase membranes coated on both sides with $La_{0.6}Sr_{0.4}CoO_{3-\delta}$.

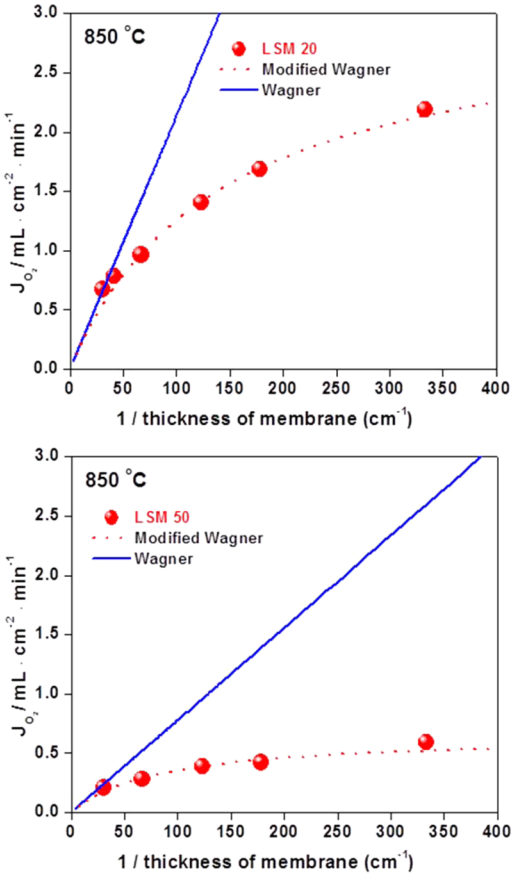

Figure 7. Oxygen permeation flux at 850 °C through LSM20 and LSM50 dual-phase membranes coated on both sides with $La_{0.6}Sr_{0.4}CoO_{3-\delta}$ as a function of the inverse of their thickness. The oxygen fluxes derived from the Wagner (solid line) and modified Wagner equations (dotted line) are also shown.

were also measured for comparison. As stated earlier, ~20 vol % is the minimum LSM concentration for electrical percolation to occur in these LSM-GDC composites.

Since the ionic conductivity of LSM (10^{-7} S·cm^{-1} at 800 °C in air)[21] is much lower than that of GDC (10^{-1} S·cm^{-1} at 800 °C in air),[26] oxygen permeation through LSM can be excluded. In order to elucidate the effects of surface modification, both or just the permeate or feed sides of the membrane were coated with LSC. The oxygen flux measured for the uncoated LSM20 membrane, 6.9×10^{-9} mol·cm^{-2}·s^{-1} at 850 °C, is low. The apparent activation energy for oxygen flux in the bare membrane was determined to be 4.25 eV, a value comparable to the activation energy for surface exchange (3.3 eV) and much higher than that for oxygen diffusion in GDC (0.6 eV).[27]

Figure 5 is a schematic representation of the possible routes for oxygen transport in GDC/LSM dual-phase membranes with

DOI: 10.1021/acsami.5b03392
ACS Appl. Mater. Interfaces 2015, 7, 14699−14707

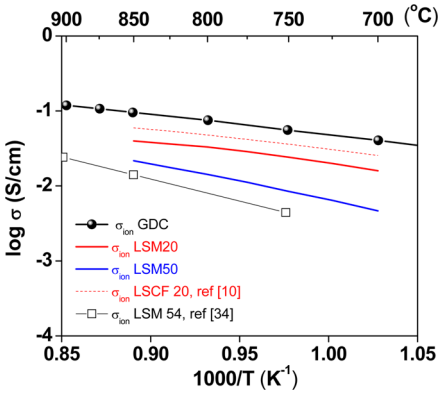

Figure 8. Temperature dependence of the oxygen ionic conductivity calculated using the modified Wagner equation for LSM20 and LSM50 dual-phase membranes coated on both sides with $La_{0.6}Sr_{0.4}CoO_{3-\delta}$.

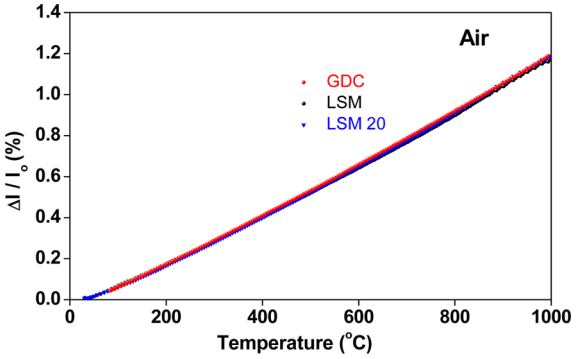

Figure 9. Dilatometric curves obtained for GDC ($Ce_{0.9}Gd_{0.1}O_{2-\delta}$), LSM ($La_{0.7}Sr_{0.3}MnO_{3\pm\delta}$), and LSM20 (80 vol % GDC−20 vol % LSM) in air.

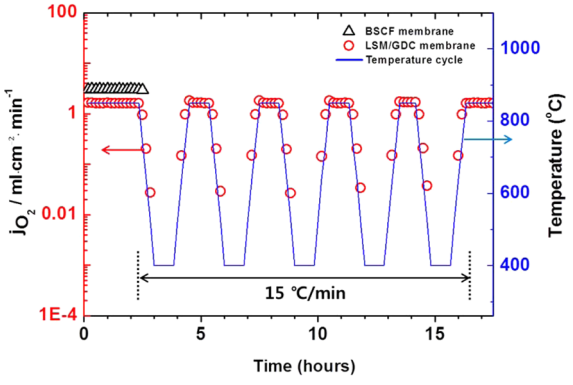

Figure 10. Oxygen permeation flux through a ∼60 μm thick LSM20 membrane and ∼100 μm thick BSCF membrane during rapid thermal cycling.

and without modification of the gas−solid interface. As mentioned previously, oxygen permeation through the LSM phase can be neglected. There are therefore only two transport paths possible through the bare membrane. Path I involves surface exchange on GDC, whereby oxygen molecules are dissociated and reduced and the resulting oxygen ion is incorporated into the bulk. This reaction has been reported to proceed slowly because of the low electrical conductivity of GDC, which also limits the supply of electrons laterally, from the percolated LSM phase. For the second possible route (path II), electrons from the percolated LSM facilitate oxygen

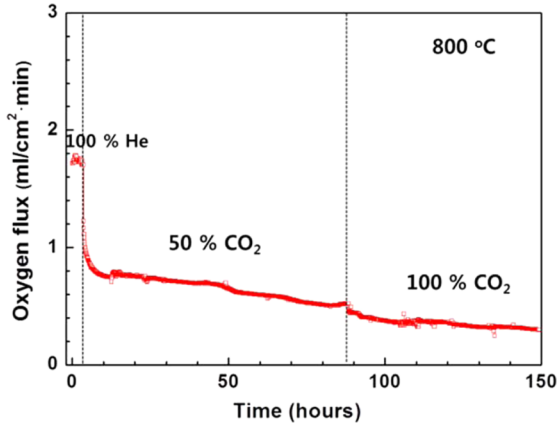

Figure 11. Oxygen permeation flux measured through a ∼60 μm thick LSM20 membrane coated on both sides with $La_{0.6}Sr_{0.4}CoO_{3-\delta}$ in a CO_2 containing atmosphere at 800 °C.

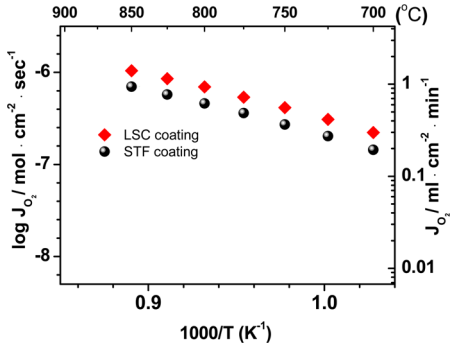

Figure 12. Temperature dependence of the oxygen permeation flux through ∼90 μm thick LSM20 dual-phase membranes coated with $La_{0.6}Sr_{0.4}CoO_{3-\delta}$ or $Sr_{0.97}Ti_{0.5}Fe_{0.5}O_{3-\delta}$.

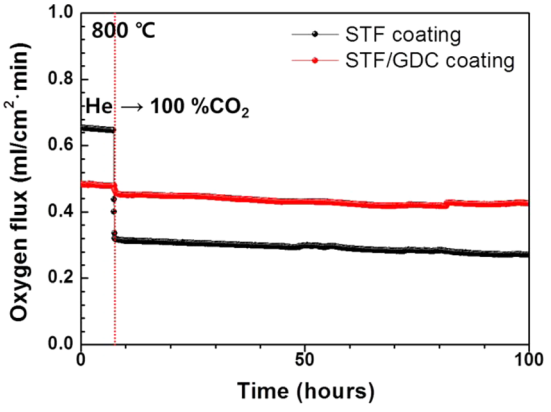

Figure 13. Oxygen permeation flux measured at 800 °C under 100% CO_2 sweep gas through ∼90 μm thick LSM20 membranes coated on both sides with either STF ($Sr_{0.97}Ti_{0.5}Fe_{0.5}O_{3-\delta}$) or an STF/$Ce_{0.9}Gd_{0.1}O_{2-\delta}$ composite.

incorporation into GDC at the triple phase boundary between the GDC, LSM, and oxygen. Since the activation energy for oxygen permeation estimated here for the bare membrane (4.25 eV) is significantly higher than the one reported in the literature for surface exchange on LSM/GDC composites (−0.19 eV),[28] this suggests that permeation via path II is negligible, or in other words, that oxygen permeation through the uncoated membrane is mostly controlled by the surface-exchange kinetics of GDC. The flux of bare pure GDC is very

DOI: 10.1021/acsami.5b03392
ACS Appl. Mater. Interfaces 2015, 7, 14699−14707

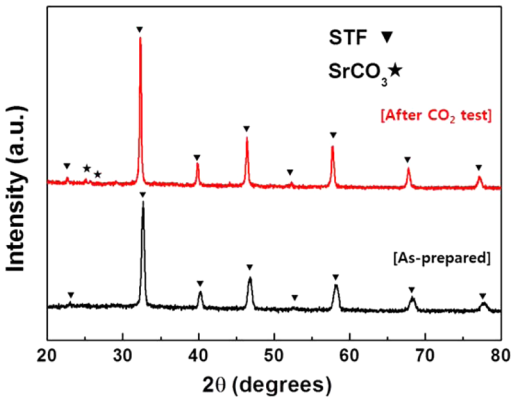

Figure 14. Room temperature X-ray patterns obtained of the STF before and after stability test under CO_2 containing atmosphere.

slightly lower than that of bare LSM20 membrane. A negligible difference of fluxes between pure GDC and LSM20 membrane clearly supports that oxygen permeation through the bare LSM20 membrane is mostly determined by the surface-exchange kinetics of GDC.

Modifying the feed-side surface of the LSM20 membrane leads to a marginal increase in the oxygen flux, but this is improved by about 1 order of magnitude by treating the permeate-side surface. This clearly indicates that different reactions govern the incorporation of oxygen on the feed side and its excorporation on the permeate side. The fact that oxygen excorporation is enhanced more substantially by surface modification suggests that this reaction, rather than incorporation, is rate limiting in this membrane. Due to the well-known decrease of the surface-exchange coefficient with decreasing of the oxygen partial pressure, surface-exchange reactions are expected to occur slowly on the permeate side. This is the possible reason for the larger improvement by modifying the permeate-side surface. Park and Choi also reported that oxygen permeation flux through YSZ (yttria-stabilized zirconia) was enhanced ~1.4 times with feed-side modification and ~4 times with permeate-side modification.[29] This result is in good agreement with our experiment results.

Coating both sides of the membrane increases the oxygen flux at 800 °C by about 3 orders of magnitude compared with the values measured for the bare membrane. The activation energy for oxygen permeation is reduced from 4.25 to 0.87 eV, indicating that the mechanism governing oxygen transport through the membrane is now ionic conduction in GDC, the activation energy of which is similar (0.61 eV). This new route is represented in Figure 5b. The electrons from the percolated LSM are readily transferred to GDC via the LSC layers, facilitating oxygen exchange reactions across the GDC surface. Electrons produced by the excorporation reaction are transferred furthermore to the percolated LSM phase. Coating both surfaces leads to the formation of an electrical short circuit through the LSM and porous LSC layers that enhances oxygen permeation through the GDC phase.

This significant increase in oxygen flux demonstrates that surface modifications of GDC/pure electronic conductor composites can alter the rate-determining reaction in the GDC phase from surface exchange to bulk diffusion. For this, tailoring the gas−solid interface on GDC is crucial to create an electrical short circuit that enhances the bulk diffusion of oxygen ions through the GDC phase of the composite. Considering the use of LSC as a SOFC cathode material, this approach could be regarded as short-circuited SOFC.

In order to further investigate the role of GDC in this dual-phase material, the oxygen flux through GDC/LSM membranes (~30 μm thick) coated on both sides with LSC was measured at 850 °C under an air/He gradient as a function of the LSM volume fraction (10−50%), as shown in Figure 6. Since the electrical percolation threshold for the LSM phase is about 20 vol %, the oxygen flux through the LSM10 membrane is relatively low (0.12 mL·cm^{-2}·min^{-1}). The oxygen flux peaks at 20 vol % LSM and gradually decreases thereafter. A composition close to the percolation threshold is therefore optimal in terms of the oxygen flux. Furthermore, the value measured here for LSM20 (2.2 mL·cm^{-2}·min^{-1} at 850 °C), is the highest ever reported for fluorite/pure electronic conductor membranes.

The oxygen flux though LSM20 and LSM50 membranes of different thicknesses (30−260 μm) was measured in order to elucidate the exchange kinetics on their surface. Since the LSM20 and LSM50 membranes are electrically percolated, the ambipolar conductivity of the membrane is determined by the ionic conductivity of GDC. If permeation is governed only by bulk diffusion, the oxygen flux follows the Wagner equation,

$$J_{O_2} \approx -\frac{RT}{16F^2L}\int_{\ln P'_{O_2}}^{\ln P''_{O_2}} \sigma_{ion}\, \mathrm{d}\ln P_{O_2} \qquad (2)$$

and the relationship between the oxygen flux and the inverse of the membrane thickness should be linear. Figure 7 shows however that this relationship is not linear for the LSM20 and LSM50 membranes, indicating that the effects of surface oxygen exchange must be taken into account.

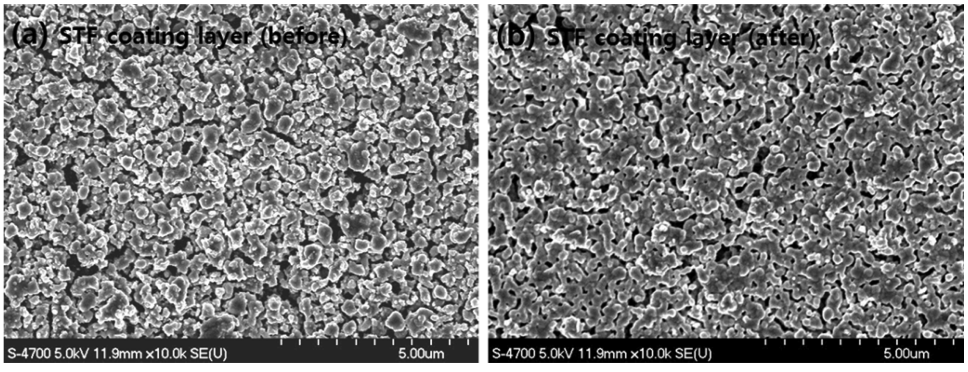

Figure 15. Microstructures of STF coating layers (a) before and (b) after permeation experiment.

DOI: 10.1021/acsami.5b03392
ACS Appl. Mater. Interfaces 2015, 7, 14699−14707

The Wagner equation can be modified as follows to account for surface-exchange kinetics:[30]

$$J_{O_2} \approx -\frac{1}{1 + (2L_C/L)} \frac{RT}{16F^2L} \int_{\ln P'_{O_2}}^{\ln P''_{O_2}} \sigma_{ion}\, d \ln P_{O_2} \quad (3)$$

where σ_{ion} is the ionic conductivity, L is the membrane thickness, L_C (=D/k, where D = diffusion coefficient and k = surface-exchange coefficient) is the characteristic thickness, and the other parameters have their usual meanings. Since the exchange reaction at the feed and permeate sides are different, L_C represents an effective or characteristic thickness. In addition, since L_C is the function of oxygen partial pressure, the calculated L_C value in this study could be only applied to the air/He gradient. The modified Wagner equation more accurately describes the thickness dependence of oxygen permeation through the LSM20 and LSM50 membranes because surface-exchange effects cannot be ignored.

Incorporating the thickness-independent parameters into a single constant simplifies eq 3 to[31]

$$J_{O_2} = \frac{1}{1 + (2L_C/L)} \frac{C}{L} = \frac{C}{L + 2L_C} \quad (4)$$

where C is the specific permeation flux at a specific oxygen partial pressure gradient and temperature. Even though C and L_C are unknown parameters, these can be calculated by fitting (here, using the nonlinear least-squares method) the data obtained for the LSM20 and LSM50 membranes. The values obtained in this way for L_C and C at 850 °C are ∼35 and ∼60 μm, and 1.6×10^{-8} and 5.8×10^{-9} mol·cm^{-1}·s^{-1}, for the LSM20 and LSM50 samples, respectively. The specific permeation flux of the LSM20 is larger than that of the LSM 50. This demonstrates that the ionic conductivity of the LSM 20 membrane is larger than that of LSM 50 membrane. Since L_C (D/k) in pure GDC is on the order of a centimeter ($D \sim 2 \times 10^{-8}$ cm^2·s^{-1}, $k \sim 3 \times 10^{-9}$ cm·s^{-1} at 800 °C),[27] these results show that surface modification leads to significant decrease in the characteristic thickness. The oxygen flux at 850 °C through coated LSM20 and LSM50 membranes is shown in Figure 7 as a function of inverse thickness. The data in Figure 7 are well-modeled by the modified Wagner equation. This demonstrates that, in this thickness range, oxygen permeation through these coated GDC/LSM dual-phase membranes is controlled by both surface-exchange kinetics and bulk diffusion. To decide the surface-exchange coefficients of the feed and permeate sides, the study of oxygen partial pressure dependence should be performed.[32,33] We will address this issue in an upcoming report.

The nominal ionic conductivity of the membrane can also be obtained using the modified Wagner equation; namely,

$$\sigma_{ion} = J_{O_2} \frac{16F^2}{RT} \left[\ln\left(\frac{P_{O_2}^{high}}{P_{O_2}^{low}} \right) \right]^{-1} (L + 2L_C) \quad (5)$$

This is increased by a factor $(L + 2L_C)/L$ compared with the conductivity derived from the original Wagner equation.

Figure 8 shows the oxygen ionic conductivity calculated using the modified Wagner equation for ∼30 μm thick LSM20 and LSM50 membranes. The ionic conductivities of LSM54[34] and LSCF20[10] membranes are also shown for comparison. Since in terms of oxygen permeation the LSM phase acts as an insulator, the ionic conductivity of the GDC/LSM composites decreases as their LSM content increases. The ionic conductivity calculated for LSM20 (0.040 S·cm^{-1} at 850 °C) is about twice that of LSM50 (0.022 S·cm^{-1} at 850 °C), indicating that an LSM content as close as possible to the percolation threshold is preferable to enhance the oxygen permeation flux. The ionic conductivity of LSM/GDC dual-phase membranes has been reported elsewhere to be much lower than that of single-phase GDC (0.014 S·cm^{-1} vs 0.10 S·cm^{-1} at 850 °C) due to the formation of a blocking layer by interphase diffusion during sintering.[35] The present study shows however that the ionic conductivity of LSM/GDC composites can be enhanced by lowering their LSM content. Taking surface-exchange kinetics into account, the ionic conductivity of the LSM20 membrane is only 60% lower than that of pure GDC (0.040 S·cm^{-1} vs 0.10 S·cm^{-1} at 850 °C). This decrease is acceptable in view of the 20 vol % LSM in the dual-phase membrane, which seems to minimize the deleterious effects on oxygen permeation of cation interdiffusion. In addition, the composite membranes in this study have ionic conductivities similar to those of GDC/LSCF membranes, demonstrating that substantial oxygen fluxes can be achieved with pure ionic/pure electronic oxide membranes.

Mechanical and Chemical Stabilities of the Dual-Phase Membrane. Figure 9 shows the linear thermal expansion rates of GDC, LSM, and LSM20. The behaviors measured for GDC and LSM are very similar to TEC values in air of 12.4×10^{-6} and 12.2×10^{-6} K^{-1}, respectively, a difference of less than 2%. In addition, since the concentration of oxygen vacancies in LSM is negligible ($\delta \approx 0$) under these conditions, the mechanical stress due to the chemical expansion of LSM can also be neglected. The mechanical stability of LSM/GDC dual-phase membranes should therefore be good under temperature fluctuations. The LSC-coated LSM20 sample was submitted to cycles of rapid heating and cooling (15 °C/min under an air/He gradient) in order to confirm the mechanical stability of the membrane. The results obtained for LSM20 are compared with those from a $Ba_{0.5}Sr_{0.5}Co_{0.8}Fe_{0.2}O_{3-\delta}$ (BSCF, thickness ∼ 100 μm) membrane with a high oxygen permeability. The TEC of BSCF is larger (>20×10^{-6} K^{-1})[16] as is its chemical expansion, making it unsuitable for rapid thermal cycling; the BCSF membrane failed during these tests. On the contrary, Figure 10 shows that the oxygen flux through the LSM20 membrane remained stable during rapid thermal cycles, demonstrating its resistance to thermal stress. It is reported that the flexural strengths of GDC and LSM at room temperature are 144[36] and 60 MPa.[37] Thus, it is expected that the ceria-based dual-phase membrane exhibits higher flexural strength than that of the single perovskite membrane. It is too difficult to measure the mechanical strength of free-standing film. The study of the mechanical strength for porous support membrane will be addressed in an upcoming report.

Figure 11 shows the oxygen flux measured through a ∼60 μm thick LSC-coated LSM20 membrane to assess its stability against CO_2 used as a sweep gas. The oxygen flux decreases significantly upon exposure to CO_2. In our previous report, the phase of LSM was stable under the presence of CO_2 atmosphere possibly due to the low SrO activity.[38] However, the LSC perovskite phase decomposes to a Ruddlesden–Popper phase (i.e., $(LaSr)_2CoO_4$) and the segregation of SrO under CO_2 exposure leads to the formation of $SrCO_3$. This reduction in the oxygen flux is therefore attributed to the instability of LSC in CO_2 atmospheres.[39−41] In order to improve the chemical stability of the coating layer, Sr(Ti,Fe)-$O_{3-\delta}$ (STF), the cobalt-free material, was used as a coating

DOI: 10.1021/acsami.5b03392
ACS Appl. Mater. Interfaces 2015, 7, 14699−14707

material instead of LSC. A site-deficient STF has indeed been reported to be highly stable under CO_2 atmospheres.[42] Since the ionic and electrical conductivity of LSC[19] are higher than those of STF[43] (0.22 S·cm^{-1} vs 0.036 S·cm^{-1}, and 160 S·cm^{-1} vs 1.8 S·cm^{-1} at 800 °C in air, respectively), the oxygen flux through the STF-coated membrane is expected to be lower. A comparison of the fluxes measured through ∼90 μm thick LSM20 dual-phase membranes coated either with LSC or STF layers is shown in Figure 12.

As expected, the oxygen flux through the membrane coated with STF is slightly lower than through the one coated with LSC. The electrochemical properties of the coating layer therefore influence the oxygen permeation fluxes achieved with these dual-phase membranes. Figure 13 presents the results of oxygen permeation experiments performed under a pure CO_2 atmosphere in order to compare the stability of LSM20 membranes coated with either pure STF or an STF/GDC (50 vol % each) composite.

The oxygen flux through the STF-coated membrane decreases abruptly upon switching the sweep gas from He to CO_2. This may be due to CO_2 adsorption on the surface hindering oxygen exchange reactions. The oxygen flux then decreases continuously under pure CO_2, probably due to the formation of $SrCO_3$. Indeed, small amounts of $SrCO_3$ were detected by XRD in the STF at the end of these tests as shown in Figure 14. The porous STF layer became slightly dense after permeation experiment as shown in Figure 15. The sintering of STF particles reduces the surface area of the coating layer and thus can decrease the surface-exchange reaction.

In contrast, the decrease in flux is mitigated by the GDC/STF coat; the composite-coated membrane exhibits a higher oxygen permeation flux under pure CO_2. The addition of GDC to the coating material therefore enhances the stability of the membrane against CO_2. Even though CO_2-tolerant membranes with a perovskite structure have been reported, few of these remain stable below 850 °C. These results show that dual-phase membranes consisting of ceria and a pure electronic conductor and coated with a Co-free material are both chemically and thermally stable and therefore constitute an important step toward the practical application of oxygen ceramic membranes.

4. CONCLUSION

Dual-phase membranes consisting of ceria and a pure electronic conductor (GDC and LSM, respectively) were prepared with different coatings and conductor phase contents, with oxygen fluxes as high 2.2 mL·cm^{-2}·min^{-1} at 850 °C measured for the LSC-coated LSM20 membrane (80 vol % GDC−20 vol % LSM, ∼30 μm thick), which is the highest oxygen permeation value ever reported for fluorite/pure electronic conductor membranes. The minimum LSM content of the composite for electrical percolation was estimated to be ∼20 vol %. The ionic conductivity of the LSM20 membrane is only ∼60% lower than that of pure GDC, indicating that the interdiffusion of the constituents during sintering is not significant. This dual-phase membrane is mechanically stable under temperature fluctuations due to the negligible difference between the TECs of the constituents. When coated with a Co-free material furthermore, the membrane delivers a relatively stable oxygen flux under a pure CO_2 atmosphere. These promising results highlight the potential of dual-phase ceria/pure-electronic-phase membranes for industrial applications.

AUTHOR INFORMATION

Corresponding Authors

*(J.H.J.) E-mail: jhjoo@kier.re.kr; jonghoonjoo@gmail.com. Tel.: 82-42-860-3132. Fax: 82-42-860-3133.

*(J.H.Y.) E-mail: jhyu@kier.re.kr.

Present Address

[§]Energy Storage Materials Research Center, Research Industrial Institute of Science and Technology, 67 Cheongam-ro, Nam-gu, Pohang, Gyeongbuk 790-330, Republic of Korea.

Notes

The authors declare no competing financial interest.

ACKNOWLEDGMENTS

This work was conducted under the framework of the Research and Development Program of the Korea Institute of Energy Research (KIER; Grant B5-2470).

REFERENCES

(1) Leo, A.; Liu, S.; Diniz da Costa, J. C. Development of Mixed Conducting Membranes for Clean Coal Energy Delivery. *Int. J. Greenhouse Gas Control* **2009**, *3*, 357−367.

(2) Merkel, T.; Lin, H.; Wei, X.; Baker, R. Power Plant Post-Combustion Carbon Dioxide Capture: An Opportunity for Membranes. *J. Membr. Sci.* **2010**, *359*, 126−139.

(3) Kneer, R.; Toporov, D.; Förster, M.; Christ, D.; Broeckmann, C.; Pfaff, E.; Zwick, M.; Engels, S.; Modigell, M. OXYCOAL-AC: Towards an Integrated Coal-Fired Power Plant Process with Ion Transport Membrane-Based Oxygen Supply. *Energy Environ. Sci.* **2010**, *3*, 198−207.

(4) Thursfield, A.; Rossiny, J. C. H.; Fearn, S.; Kilner, J. A.; Metcalfe, I. S. A Combinatorial Approach to Synthesis of the $La_{0.8}Sr_{0.2}Co_{1-y}Mn_yO_{3\pm\delta}$ Family of Perovskite-Type Mixed Conducting Metal Oxides and Characterisation of the Surface Oxygen Mobility. *Solid State Ionics* **2012**, *225*, 182−185.

(5) Han, D. Z.; Tan, X. Y.; Yan, Z. F.; Li, Q.; Liu, S. M. New Morphological $Ba_{0.5}Sr_{0.5}Co_{0.8}Fe_{0.2}O_{3-\alpha}$ Hollow Fiber Membranes with High Oxygen Permeation Fluxes. *Ceram. Int.* **2013**, *39*, 431−437.

(6) Yi, J.; Schroeder, M.; Weirich, T.; Mayer, J. Behavior of Ba(Co, Fe, Nb)$O_{3-\alpha}$ Perovskite in CO_2-Containing Atmospheres: Degradation Mechanism and Materials Design. *Chem. Mater.* **2010**, *22*, 6246−6253.

(7) Waindich, A.; Möbius, A.; Müller, M. Corrosion of $Ba_{1-x}Sr_xCo_{1-y}Fe_yO_{3-\delta}$ and $La_{0.3}Ba_{0.7}Co_{0.2}Fe_{0.8}O_{3-\delta}$ Materials for Oxygen Separating Membranes under Oxycoal Conditions. *J. Membr. Sci.* **2009**, *337*, 182−187.

(8) Arnold, M.; Wang, H.; Feldhoff, A. Influence of CO_2 on the Oxygen Permeation Performance and the Microstructure of Perovskite-Type $(Ba_{0.5}Sr_{0.5})(Co_{0.8}Fe_{0.2})O_{3-\delta}$ Membranes. *J. Membr. Sci.* **2007**, *293*, 44−52.

(9) Balaguer, M.; Garcia-Fayos, J.; Solís, C.; Serra, J. M. Fast Oxygen Separation Through SO_2- and CO_2-Stable Dual-Phase Membrane Based on $NiFe_2O_4$−$Ce_{0.8}Tb_{0.2}O_{2-\delta}$. *Chem. Mater.* **2013**, *25*, 4986−4993.

(10) Joo, J. H.; Yun, K. S.; Lee, Y.; Jung, J.; Yoo, C.-Y.; Yu, J. H. Dramatically Enhanced Oxygen Fluxes in Fluorite-Rich Dual-Phase Membrane by Surface Modification. *Chem. Mater.* **2014**, *26*, 4387−4394.

(11) Liang, F.; Luo, H.; Partovi, K.; Ravkina, O.; Cao, Z.; Liu, Y.; Caro, J. A Novel CO_2-Stable Dual Phase Membrane with High Oxygen Permeability. *Chem. Commun. (Cambridge, U. K.)* **2014**, *50*, 2451−2454.

(12) Fang, W.; Liang, F.; Cao, Z.; Steinbach, F.; Feldhoff, A. A Mixed Ionic and Electronic Conducting Dual-Phase Membrane with High Oxygen Permeability. *Angew. Chem., Int. Ed.* **2015**, *54*, 1−5.

(13) Ruiz-Trejo, E.; Boldrin, P.; Lubin, A.; Tariq, F.; Fearn, S.; Chater, R.; Cook, S. N.; Atkinson, A.; Gruar, R. I.; Tighe, C. J.; Darr,

DOI: 10.1021/acsami.5b03392
ACS Appl. Mater. Interfaces 2015, 7, 14699−14707

J.; Brandon, N. P. Novel Composite Cermet for Low-Metal-Content Oxygen Separation Membranes. *Chem. Mater.* **2014**, *26*, 3887−3895.
(14) Cao, Z.; Zhu, X.; Li, W.; Xu, B.; Yang, L.; Yang, W. Asymmetric Dual-Phase Membranes Prepared via Tape-Casting and Co-Lamination for Oxygen Permeation. *Mater. Lett.* **2015**, *147*, 88−91.
(15) Xue, J.; Liao, Q.; Wei, Y.; Li, Z.; Wang, H. A CO_2-Tolerance Oxygen Permeable $60Ce_{0.9}Gd_{0.1}O_{2-\delta}$-$40Ba_{0.5}Sr_{0.5}Co_{0.8}Fe_{0.2}O_{3-\delta}$ Dual Phase Membrane. *J. Membr. Sci.* **2013**, *443*, 124−130.
(16) Wei, B.; Lü, Z.; Li, S.; Liu, Y.; Liu, K.; Su, W. Thermal and Electrical Properties of New Cathode Material $Ba_{0.5}Sr_{0.5}Co_{0.8}Fe_{0.2}O_{3-\delta}$ for Solid Oxide Fuel Cells. *Electrochem. Solid-State Lett.* **2005**, *8*, 428−431.
(17) Jiang, S. P. Development of Lanthanum Strontium Manganite Perovskite Cathode Materials of Solid Oxide Fuel Cells: A Review. *J. Mater. Sci.* **2008**, *43*, 6799−6833.
(18) Mogensen, M.; Lindegaard, T.; Hansen, U. R.; Mogensen, G. Physical Properties of Mixed Conductor Solid Oxide Fuel Cell Anodes of Doped CeO_2. *J. Electrochem. Soc.* **1994**, *141*, 2122−2128.
(19) Ullmann, H.; Trofimenko, N.; Tietz, F.; Stöver, D.; Ahmad-Khanlou, A. Correlation between Thermal Expansion and Oxide Ion Transport in Mixed Conducting Perovskite-Type Oxides for SOFC Cathodes. *Solid State Ionics* **2000**, *138*, 79−90.
(20) Kharton, V. V.; Kovalevsky, A. V.; Viskup, A. P.; Figueiredo, F. M.; Yaremchenko, A. A.; Naumovich, E. N.; Marques, F. M. B. Oxygen Permeability of $Ce_{0.8}Gd_{0.2}O_{2-\delta}$-$La_{0.7}Sr_{0.3}MnO_{3-\delta}$ Composite Membranes. *J. Electrochem. Soc.* **2000**, *147*, 2814−2821.
(21) Fleig, J.; Kim, H.-R.; Jamnik, J.; Maier, J. Oxygen Reduction Kinetics of Lanthanum Manganite (LSM) Model Cathodes: Partial Pressure Dependence and Rate-Limiting Steps. *Fuel Cells* **2008**, *8*, 330−337.
(22) McLachlan, D. S.; Blaszkiewicz, M.; Newnham, R. E. Electrical Resistivity of Composites. *J. Am. Ceram. Soc.* **1990**, *73*, 2187−2203.
(23) Han, D. G.; Choi, G. M. Computer Simulation of the Electrical Conductivity of Composites: the Effect of Geometrical Arrangement. *Solid State Ionics* **1998**, *106*, 71−87.
(24) Seeharaj, P.; Berenov, A.; Raj, E.; Rudkin, R.; Atkinson, A. Mixed-Conducting LSC/CGO Composites for Passive Oxygen Separation Membranes. *Solid State Ionics* **2011**, *192*, 638−641.
(25) Shaula, A. L.; Kharton, V. V.; Marques, F. M. B.; Kovalevsky, A. V.; Viskup, A. P.; Naumovich, E. N. Oxygen Permeability of Mixed-Conducting Composite Membranes: Effects of Phase Interaction. *J. Solid State Electrochem.* **2006**, *10*, 28−40.
(26) Joo, J. H.; Choi, G. M. Electrical Conductivity of Thin Film Ceria Grown by Pulsed Laser Deposition. *J. Eur. Ceram. Soc.* **2007**, *27*, 4273−4277.
(27) Lane, J. A.; Kilner, J. A. Oxygen Surface Exchange on Gadolinia Doped Ceria. *Solid State Ionics* **2000**, *136−139*, 927−932.
(28) Armstrong, E. N.; Duncan, K. L.; Wachsman, E. D. Surface Exchange Coefficients of Composite Cathode Materials Using in Situ Isothermal Isotope Exchange. *J. Electrochem. Soc.* **2011**, *158*, 283−289.
(29) Park, H. J.; Choi, G. M. Oxygen Exchange and Transport Properties of Yttria-Stabilized Zirconia Coated with $LaCrO_3$. *J. Electroceram.* **2006**, *17*, 781−786.
(30) Bouwmeester, H. J. M.; Kruidhof, H.; Burggraaf, A. J. Importance of the Surface Exchange Kinetics as Rate Limiting Step in Oxygen Permeation through Mixed-Conducting Oxides. *Solid State Ionics* **1994**, *72*, 185−194.
(31) Joo, J. H.; Park, G. S.; Yoo, C.-Y.; Yu, J. H. Contribution of the Surface Exchange Kinetics to the Oxygen Transport Properties in $Gd_{0.1}Ce_{0.9}O_{2-\delta}$−$La_{0.6}Sr_{0.4}Co_{0.2}Fe_{0.8}O_{3-\delta}$ Dual-Phase Membrane. *Solid State Ionics* **2013**, *253*, 64−69.
(32) Zhu, X.; Yang, W. Composite Membrane Based on Ionic Conductor and Mixed Conductor for Oxygen Permeation. *AIChE J.* **2008**, *54*, 665−672.
(33) Zhu, X.; Liu, H.; Cong, Y.; Yang, W. Permeation Model and Experimental Investigation of Mixed Conducting Membranes. *AIChE J.* **2012**, *58*, 1744−1754.
(34) Kharton, V. V.; Kovalevsky, A. V.; Viskup, A. P.; Shaula, A. L.; Figueiredo, F. M.; Naumovich, E. N.; Marques, F. M. B. Oxygen Transport in $Ce_{0.8}Gd_{0.2}O_{2-\delta}$-Based Composite Membranes. *Solid State Ionics* **2003**, *160*, 247−258.
(35) Kharton, V. V.; Kovalevsky, A. V.; Viskup, A. P.; Figueiredo, F. M.; Yaremchenko, A. A.; Naumovich, E. N.; Marques, F. M. B. Oxygen Permeability and Faradaic Efficiency of $Ce_{0.8}Gd_{0.2}O_{2-\delta}$−$La_{0.7}Sr_{0.3}MnO_{3-\delta}$ Composites. *J. Eur. Ceram. Soc.* **2001**, *21*, 1763−1767.
(36) Nakajo, A.; Kuebler, J.; Faes, A.; Vogt, U. F.; Schindler, H. J.; Chiang, L.-K.; Modena, S.; Van herle, J.; Hocker, T. Compilation of Mechanical Properties for the Structural Analysis of Solid Oxide Fuel Cell Stacks. Constitutive Materials of Anode-Supported Cells. *Ceram. Int.* **2012**, *38*, 3907−3927.
(37) Trunec, M. Fabrication of Zirconia- and Ceria- Based Thin-Wall tubes by Thermoplastic Extrusion. *J. Eur. Ceram. Soc.* **2004**, *24*, 645−651.
(38) Yun, K. S.; Yoo, C.-Y.; Yoon, S.-G.; Yu, J. H.; Joo, J. H. Chemically and Thermo-Mechanically stable LSM−YSZ Segmented Oxygen Permeable Ceramic Membrane. *J. Mater. Sci.* **2015**, *486*, 222−228.
(39) Hashimoto, S.; Fukuda, Y.; Kuhn, M.; Sato, K.; Yashiro, K. Oxygen Nonstoichiometry and Thermo-Chemical Stability of $La_{0.6}Sr_{0.4}Co_{1-y}Fe_yO_{3-\delta}$ (y=0.2, 0.4, 0.6, 0.8). *Solid State Ionics* **2010**, *181*, 1713−1719.
(40) Esposito, V.; Søgaard, M.; Hendriksen, P. V. Chemical Stability of $La_{0.6}Sr_{0.4}CoO_{3-\delta}$ in Oxygen Permeation Applications under Exposure to N_2 and CO_2. *Solid State Ionics* **2012**, *227*, 46−56.
(41) Morales, M.; Espiell, F.; Segarra, M. Performance and Stability of $La_{0.5}Sr_{0.5}CoO_{3-\delta}$ Perovskite as Catalyst Precursor for Syngas Production by Partial Oxidation of Methane. *Int. J. Hydrogen Energy* **2014**, *39*, 6454−6461.
(42) Kharton, V. V.; Kovalevsky, A. V.; Tsipis, E. V.; Viskup, A. P.; Naumovich, E. N.; Jurado, J. R.; Frade, J. R. Mixed Conductivity and Stability of A-Site-Deficient $Sr(Fe,Ti)O_{3-\delta}$ Perovskites. *J. Solid State Electrochem.* **2002**, *7*, 30−36.
(43) Jung, W.; Tuller, H. L. Impedance Study of $SrTi_{1-x}FexO_{3-\delta}$ (x = 0.05 to 0.80) Mixed Ionic-Electronic Conducting Model Cathode. *Solid State Ionics* **2009**, *180*, 843−847.

DOI: 10.1021/acsami.5b03392
ACS Appl. Mater. Interfaces 2015, 7, 14699−14707